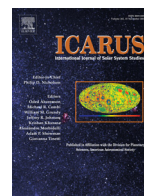




ELSEVIER

Contents lists available at ScienceDirect

Icarus

journal homepage: www.elsevier.com/locate/icarus

Porosity effects on crystallization kinetics of amorphous solid water: Implications for cold icy objects in the outer solar system

Emily H. Mitchell^{a,*}, Ujjwal Raut^b, Benjamin D. Teolis^b, Raúl A. Baragiola^{a,1}

^aLaboratory for Astrophysics and Surface Physics, Thornton Hall B 113, University of Virginia, Charlottesville, VA 22904, United States

^bSouthwest Research Institute, Space Science and Engineering Division, 6220 Culebra Road, San Antonio, TX 78238, United States

ARTICLE INFO

Article history:

Received 6 July 2016

Revised 15 October 2016

Accepted 4 November 2016

Available online xxx

Keywords:

Ices, IR spectroscopy

Ices, UV spectroscopy

Satellites, surfaces

Europa

Thermal histories

ABSTRACT

We have investigated the effects of porosity on the crystallization kinetics of amorphous solid water (ASW). Porosity in ASW films, condensed from the vapor phase at varying incidences at 10 K, was characterized using ultraviolet-visible interferometry and quartz crystal microgravimetry. The films were heated to crystallization temperatures between 130 and 141 K, resulting in partial pore compaction. The isothermal phase transformation was characterized using transmission infrared spectroscopy to monitor the time evolution of the 3.1- μm O–H stretch absorption band. We find that ASW crystallization unfolds in two distinct stages. The first stage, responsible for $\sim 10\%$ transformation, is initiated from nucleation at the external surface. The dominant second stage begins with nucleation at the internal pore surfaces and completes the transformation of the film at a faster rate compared to the first stage. A key finding is that porosity has major influence on crystallization kinetics; a film with five-times-higher porosity was observed to crystallize ~ 15 times faster, compared to the less porous counterpart. We extrapolate our results to predict crystallization times for amorphous ices condensed on Europa's surface from plume sources, as recently observed by the Hubble Space Telescope.

© 2016 Elsevier Inc. All rights reserved.

1. Introduction

Crystalline water ice is pervasive on many cold objects in the Outer Solar System. The near-infrared spectrum of Charon's surface from the 2015 *New Horizons* flyby shows the 1.65- μm absorption band (Cruikshank et al., 2015; Grundy et al., 2016), diagnostic of crystalline ice (Schmitt et al., 1998). Other Kuiper Belt objects (KBOs) or trans-Neptunian objects (TNOs), like Haumea (Merlin et al., 2007) and Quaoar (Jewitt and Luu, 2004), are also known to have crystalline ice, despite surface temperatures < 50 K. Crystalline ice is also found on the surfaces of most Jovian and Saturnian satellites (Grundy et al., 1999), where temperatures are usually less than 130 K. For instance, a recent study based on spectral modeling of the 1.65- μm absorption from SINFONI observations estimate the average global amorphous-to-crystalline ice ratio on Europa to be 0.57 ± 0.25 (Ligier et al., 2016).

The presence of crystalline ice on these cold objects is puzzling, since laboratory studies show that ice films condensed from vapor at temperatures < 130 K results only in the amorphous phase

(Sceats and Rice, 1982). Amorphous ice can form on the surfaces of cold astronomical objects from either condensation of sputtered molecules or vapor from plume sources, as observed on Enceladus (Hansen et al., 2006; Waite et al., 2006) and Europa (Roth et al., 2014a), returning in gravitationally-determined trajectories. Since amorphous ice is metastable, it will transform to the thermodynamically-stable cubic crystalline phase at a temperature-dependent rate. However, the transformation is extremely slow at colder temperatures, likely requiring ~ 10 million years at 80 K (Baragiola, 2003). Furthermore, the icy surfaces are continually bombarded by energetic particles and photon irradiation. Laboratory studies have shown that such energetic irradiation can amorphize crystalline ice, and more efficiently below 80 K, thereby reversing any thermally-driven crystallization on the cold surfaces of satellites and TNOs (Baratta et al., 1991; Moore and Hudson, 1992; Kouchi and Kuroda, 1990; Strazzulla et al., 1992; Leto and Baratta, 2003; Famá et al., 2010).

A salient feature of vapor-deposited ASW films is its porosity, which increases with incidence of the vapor flux (Stevenson et al., 1999) and is known to affect other properties of amorphous ice such as gas retention capacity, mechanical strength, and thermal conductivity, among others (Baragiola, 2003). Irradiating ice films with energetic particles reduces the porosity, i.e. compaction

* Corresponding author.

E-mail address: ehm4qb@virginia.edu (E.H. Mitchell).

¹ Deceased

(Raut et al., 2007a, 2008; Mejía et al., 2015), as does thermal heating (Johari et al., 1991; Giering and Haarer, 1996; Tsekouras et al., 1998; Bossa et al., 2012; Isokoski et al., 2014). Whether porosity can alter the crystallization kinetics of ASW films remains an open question, although such effects have been observed in other solids such as zeolites (Frances and O'Hare, 1998) and titania (Kirsch et al., 2004).

Previous studies have shown that crystallization is initiated at the external surface of a thin non-porous film, where the nucleation barrier is reduced (Lofgren et al., 1996; Backus et al., 2004). This was attributed to the presence of surficial water molecules that can be easily rearranged into ordered, crystalline nuclei, compared to the tetrahedrally-bonded bulk molecules. Since porous ice films present large internal surface area, \sim hundreds of $\text{m}^2 \text{g}^{-1}$, they largely exceed non-porous films in the number of possible nucleation sites. Therefore, porosity is expected to enhance crystallization rates in ASW films. However, crystallization times in porous ASW and compact hyperquenched ice films showed no significant difference, despite seven-fold difference in surface area (Maté et al., 2012). Additionally, the onset site of crystallization in ASW films is still debated, with other studies reporting that formation of crystalline nuclei is more favored in the bulk rather than at the surfaces (Rowland et al., 1995; Buch et al., 1996; Kondo et al., 2007).

Here, we report on isothermal crystallization of vapor-deposited amorphous solid water with varying porosities over 130–141 K. The porosity of the ASW films is controlled at growth by changing the deposition incidence angle of the water vapor flux. We measure the dependence of crystallization rates and activation energy on porosity. We then extrapolate our results to lower temperatures to predict porosity-dependent crystallization times on cold extraterrestrial surfaces.

2. Experimental setup

The experiments were performed in an ultra-high vacuum (UHV) chamber cryopumped to a base pressure of $\sim 10^{-10}$ Torr. Water ice films were vapor-deposited onto a CsI substrate cooled to 10 K by a two-stage Janis RDK-205E closed-cycle refrigerator; these growth conditions result in microporous ASW (Sceats and Rice, 1982). An alkali halide substrate, as used in this work, makes optical analysis simpler since interference effects are minor in transmission compared to reflectance geometry (Teolis et al., 2007). Furthermore, an insulator substrate is an improved analog of icy satellite surfaces over metallic substrates previously used in several other studies (Dohnálek et al., 2000; Sack and Baragiola, 1993; Lofgren et al., 2003; Safarik et al., 2003; Smith et al., 2011).

The deposition angle of the collimated vapor flux from a micro-capillary array (MCA) doser was varied from 0° to 70° with respect to the normal. In some instances, ice films were deposited from an omnidirectional vapor source. Films deposited from collimated fluxes will henceforth be referred to by their deposition angles (for instance, a 45° film) and the omnidirectionally-deposited films will be referred to as background-deposited ice (BDI). To prevent accumulation of ice on both sides of the CsI substrate, the side facing away from the doser was fitted with a cooled hollow shielding tube that blocks $\sim 97\%$ of the water vapor flux from reaching the rear of the CsI substrate, while still allowing optical transmission.

The ice density ρ was calculated from the ratio of η to d , where η is the column density of the ice film deposited on the CsI substrate and d is the film thickness. To estimate η on the CsI substrate, we performed a separate calibration experiment using a piezoelectric quartz crystal microbalance (QCM), mounted 25.4 mm above the CsI substrate in the cryogenically-cooled sample holder. The QCM is highly sensitive, able to detect accretion of $\sim 0.1 \text{ H}_2\text{O ML}$ ($1 \text{ ML} = 10^{15} \text{ mol cm}^{-2}$, about a monolayer).

We began the calibration experiment by measuring the deposition rate R_{QCM} with the MCA doser and the QCM on the same vertical plane. The sample holder was then vertically translated with respect to the MCA doser, and we monitored the change in deposition rate measured by the QCM until the doser was facing the CsI substrate. The collimation of the water vapor flux effusing from the MCA doser has a forward cosine distribution (Winkler and Yates, 1988), and the QCM thus intercepts a fraction of the vapor flux directed toward the CsI substrate, $\sim 20\%$ in our setup. The deposition rate measured by the QCM when the doser is positioned to face the CsI substrate is denoted R_{CsI} , and it is related to R_{QCM} by $\alpha = R_{\text{QCM}}/R_{\text{CsI}}$.

We ensure that the H_2O pressure, measured with a nude ionization gauge, is kept constant to within $\sim 10\%$ during the vertical translation. We also assumed the sticking coefficient of water molecules impinging on the QCM and CsI substrates to be ~ 1 at 10 K.

In subsequent experiments with the water vapor flux directed toward the CsI substrate for time t , we measure R_{CsI} in real-time and determine η using

$$\eta = R_{\text{CsI}} \times t \times \alpha \quad (1)$$

The film thickness d was derived by fitting the Fresnel equations to the interference pattern in the optical transmission in the ultraviolet (UV)-visible range (Westley et al., 1998; Heavens, 1991; Raut et al., 2008). Using 0.94 g cm^{-3} for the density of compact ice ρ_c (Narten et al., 1976), we obtained the porosity ($\Phi = 1 - \rho/\rho_c$) of the ice films. Our method for estimating η from QCM calibration experiments yielded errors in Φ of ± 0.03 (~ 5 to 20%) for all H_2O incidence angles, larger than the ± 0.01 error inherent in the calculation of d from the fit of the interference pattern.

The films were also characterized by transmission Fourier transform infrared spectrometry (FTIR) at 2 cm^{-1} resolution using a Thermo Nicolet Nexus 670 spectrometer thoroughly purged with dry air. The spectra T of the films were divided by the transmission spectrum T_0 of the bare CsI window and then converted to optical depth, $-\ln(T/T_0)$. In particular, we focused on the changes of the O–H-stretch absorption band ($3.1 \mu\text{m}$) and the O–H dangling bond (DB) absorption features at $\sim 2.7 \mu\text{m}$, due to heating and isothermal annealing at higher temperatures.

3. Results

3.1. Porosity in ASW films

Fig. 1A shows infrared absorption spectra in the region of the dangling O–H bands ($\sim 2.7 \mu\text{m}$) of ice films deposited at 10 K at different incidences. The absorption features, DB1 (3270 cm^{-1}) and DB2 (3696 cm^{-1}), are assigned to O–H vibrations of doubly- and triply-coordinated surface water molecules, respectively (Rowland and Devlin, 1991), and are diagnostic of pore-related internal surface area (Devlin and Buch, 1995; Raut et al., 2007b). Fig. 1B shows transmittance spectra (black curves) of ice films deposited at 10 K at 0° , 45° , and 70° incidences, together with fits (red curves) to the Fresnel equations (Heavens, 1991). The oscillating pattern in the spectra is due to optical interference between directly transmitted light and light transmitted following multiple reflections at different interfaces. The ice layer serves as an anti-reflection coating, increasing the transmitted light intensity compared to that of the bare CsI substrate, i.e. $T > 1$. The film thickness d obtained from the fits, together with column density η determined from the microbalance calibration experiment, gives the initial ice porosity Φ_0 , which increases with incidence angle from 0.16 (0°) to 0.51 (70°). We have also included an infrared spectrum of a BDI film in Fig. 1A. We find that BDI and 45° films have, within errors, similar integrated DB absorption band area ($0.24 \pm 0.01 \text{ cm}^{-1}$) and porosity

Download English Version:

<https://daneshyari.com/en/article/5487072>

Download Persian Version:

<https://daneshyari.com/article/5487072>

[Daneshyari.com](https://daneshyari.com)